

RECOVERING CONDUCTIVITY AT THE BOUNDARY IN THREE-DIMENSIONAL ELECTRICAL IMPEDANCE TOMOGRAPHY

GEN NAKAMURA¹, PÄIVI RONKANEN², SAMULI SILTANEN³ AND KAZUMI TANUMA⁴

ABSTRACT. The aim of electrical impedance tomography (EIT) is to reconstruct the conductivity values inside a conductive object from electric measurements performed at the boundary of the object. EIT has applications in medical imaging, nondestructive testing, geological remote sensing and subsurface monitoring. Recovering the conductivity and its normal derivative at the boundary is a preliminary step in many EIT algorithms; Nakamura and Tanuma introduced formulae for recovering them approximately from localized voltage-to-current measurements in [Recent Development in Theories & Numerics, International Conference on Inverse Problems 2003]. The present study extends that work both theoretically and computationally. As a theoretical contribution, reconstruction formulas are proved in a more general setting. On the computational side, numerical implementation of the reconstruction formulae is presented in three-dimensional cylindrical geometry. These experiments, based on simulated noisy EIT data, suggest that the conductivity at the boundary can be recovered with reasonable accuracy using practically realizable measurements. Further, the normal derivative of the conductivity can also be recovered in a similar fashion if measurements from a homogeneous conductor (dummy load) are available for use in a calibration step.

Version 11, November 9, 2009

1. INTRODUCTION

The aim of Electrical Impedance Tomography (EIT) is imaging the conductivity distribution inside an unknown body from electrical measurements at the boundary. Applications of EIT include medical imaging, nondestructive testing and subsurface monitoring, see [4, 5, 9]. We introduce a new practical solution method for the subproblem of recovering the conductivity and its normal derivative at the boundary of a three-dimensional target from localized measurements. This is required in several EIT algorithms as the first step before full reconstruction.

Assume given a bounded domain $\Omega \subset \mathbb{R}^3$ with Lipschitz boundary $\partial\Omega$ and a strictly positive real-valued conductivity $\gamma \in L^\infty(\Omega)$. We consider applying a voltage potential f on the boundary and solving the Dirichlet problem

$$(1.1) \quad \begin{cases} \nabla \cdot (\gamma \nabla u) = 0 & \text{in } \Omega, \\ u = f & \text{on } \partial\Omega, \end{cases}$$

where $u = u(x)$ is electric potential. The resulting distribution of current through the boundary is

$$(1.2) \quad \Lambda_\gamma f = \gamma \frac{\partial u}{\partial \nu} \Big|_{\partial\Omega}$$

where Λ_γ is the Dirichlet-to-Neumann (DN) map and ν is the outward unit normal. The problem is to determine γ from the knowledge of Λ_γ . This mathematical formulation was introduced by Calderón in [8].

Practical measurements are typically done using a finite number of electrodes on the surface of the body, and various data models including electrodes are discussed in [10, 36]. In this study we use the *continuum model* (1.1) for simplicity. However, the effect of electrodes is taken into account by considering the maximum frequency of spatial oscillations in Dirichlet data f in (1.1) that can be approximated with reasonable accuracy using a given number of electrodes.

The following cylindrical geometry is frequently used in our discussion. Take $\ell > 0$ and $R > 0$ and define

$$(1.3) \quad \Omega := \{(x_1^2 + x_2^2)^{1/2} < R, |x_3| < \ell\} = \Omega' \times [-\ell, \ell] \subset \mathbb{R}^3,$$

where $\Omega' = D(0, R) \subset \mathbb{R}^2$. Denote the lateral boundary surface of Ω by

$$\Gamma := \{(x_1^2 + x_2^2)^{1/2} = R, |x_3| < \ell\} = (\partial\Omega') \times [-\ell, \ell] \subset \partial\Omega.$$

Parametrize a neighborhood of Γ by boundary normal coordinates (τ, s, r) :

$$(1.4) \quad x_1 = (R - r) \cos(s/R), \quad x_2 = (R - r) \sin(s/R), \quad x_3 = \tau.$$

Then Ω and Γ are given by $0 < r \leq R$ and $r = 0$, respectively.

Given a point $x_0 \in \Gamma$, we wish to recover $\gamma(x_0)$ and $\partial\gamma/\partial\nu(x_0)$ approximately from the (local) knowledge of Λ_γ . Without loss of generality we may put $x_0 = (0, 0, 0)$ in the coordinate system (τ, s, r) . We assume that the conductivity γ is twice continuously differentiable in a neighborhood of the boundary. Let $\eta(\tau, s)$ be any function in $C_0^1(\Gamma)$, choose a unit vector $(t_1, t_2) \in \mathbb{R}^2$ and define

$$(1.5) \quad \phi_N(\tau, s) = e^{iN(\tau t_1 + s t_2)} \eta(\tau, s),$$

$$(1.6) \quad \psi_N(\tau, s) = e^{i\frac{N}{2}(\tau t_1 + s t_2)} \eta(\tau, s).$$

The following formulas can be derived from Theorem 1 in Section 2:

$$(1.7) \quad \int_{\mathbb{R}^2} \gamma(\tau, s, 0) \eta(\tau, s)^2 d\tau ds = \lim_{N \rightarrow \infty} N^{-1} \langle \Lambda_\gamma \phi_N, \overline{\phi_N} \rangle,$$

$$(1.8) \quad \int_{\mathbb{R}^2} \frac{\partial\gamma}{\partial\nu}(\tau, s, 0) \eta(\tau, s)^2 d\tau ds = \lim_{N \rightarrow \infty} \left[\left(2 - \frac{1 + t_1^2 - t_2^2}{2RN} \right) \langle \Lambda_\gamma \phi_N, \overline{\phi_N} \rangle - 4 \langle \Lambda_\gamma \psi_N, \overline{\psi_N} \rangle \right].$$

Practical implementation of formulas (1.7) and (1.8) in dimension two is reported in [33]; according to those results, formula (1.7) can be used reliably for approximate recovery of the conductivity at the boundary, while practical use of formula (1.8) seems to require an unrealistic number of electrodes.

This paper has two goals. The theoretical goal is to prove generalizations of formulas (1.7) and (1.8) in a more general setting, where formula (1.8) contains geometric information about the boundary $\partial\Omega$. Such information may be used for estimating the shape of the boundary from EIT data, but we do not discuss such possibilities further in this work.

The computational goal is to implement (1.7) and (1.8) numerically in the three-dimensional cylindrical geometry (1.3) and study the possibilities of using them in practical EIT. We recover the trace of conductivity approximately at the boundary using formula (1.7) with a finite value of N . The results suggest that the right hand

side of (1.7) converges as $N \rightarrow \infty$ quickly enough for the Dirichlet data (1.5) to remain only mildly oscillatory. It seems that the frequency of those oscillations is low enough for $\phi_N(\tau, s)$ to be represented reasonably accurately using 64 electrodes.

Practical use of formula (1.8) to recover the normal derivative of the conductivity seems to be more problematic, as is the case in the two-dimensional situation [33]. The convergence of the right hand side of (1.8) is too slow for acceptable reconstructions from realistic voltage-to-current measurements. However, our numerical experiments suggest that the difference between the right hand sides of (1.8) corresponding to a nontrivial conductivity and to a constant conductivity do converge rather quickly as $N \rightarrow \infty$, allowing reasonable reconstructions of normal derivative from realistic data after a calibration step.

Most three-dimensional EIT algorithms for recovering conductivity inside Ω are iterative methods where the direct problem (1.1) needs to be solved repeatedly using a numerical algorithm, typically the finite element method (FEM). This is computationally demanding since 3D FEM involves representing the conductivity with a large number of parameters. Out of the few published implementations of 3D EIT we mention the work of Barber, Brown, Metherall and Smallwood [24, 25, 26]; Blue, Goble, Cheney, Isaacson, Newell, Ross and Saulnier [3, 17, 34]; Morucci, Granie, Lei, Chabert and Marsili [27]; Kaipio, Savolainen, P.J. Vauhkonen and M. Vauhkonen [38, 39, 40]; and Wexler [41]. In all these works the reconstruction algorithms need a good initial guess for conductivity inside Ω in order to convergence to the global minimum; at present γ is often assumed to be constant near the boundary. We believe that the knowledge of conductivity γ and its normal derivative at the boundary $\partial\Omega$ helps to design better initial guesses for full reconstruction algorithms.

Non-iterative 3D EIT algorithms have been suggested as well, see [2, 6, 12], and numerical inclusion detection algorithms are presented in [18, 15, 19]. In such methods it may be important to continue the conductivity artificially outside Ω in a regular fashion; this involves recovering γ and $\partial\gamma/\partial\nu$ at the boundary first.

Previous theoretical results on the recovery of conductivity and its derivatives at the boundary include [1, 22, 23, 28, 29, 37] starting from infinite precision data measured on the whole boundary, and [7, 21, 30, 31, 32] starting from infinite precision data measured on a part of the boundary. The present work is the first numerical boundary reconstruction result in dimension three.

This paper is organized as follows. In Section 2 we give a proof of formulas (1.7) and (1.8) using our main Theorem 1, which in turn is proved in Section 3. In Section 4 we explain how we simulate noisy voltage-to-current data, and in Section 5 we substitute the data to formulas (1.7) and (1.8) to study their convergence in practice as N grows. Based on those numerical experiments we introduce and demonstrate a calibrated reconstruction method in Section 6. Finally, we conclude our findings in Section 7.

2. BASIC THEOREM AND DERIVATION OF FORMULAS (1.7) AND (1.8)

Let Ω be a bounded domain in \mathbb{R}^n with $n \geq 2$. We assume that the boundary $\partial\Omega$ is Lipschitz and, in addition, locally C^1 near a recovery point $x_0 \in \partial\Omega$. Then there exists a C^1 diffeomorphism $y = \Psi(x)$ which induces a curvilinear coordinate system $y = (y', y_n) = (y_1, \dots, y_{n-1}, y_n)$ around x_0 such that $\Psi(x_0) = 0$ and $\Omega, \partial\Omega$

are given by

$$(2.1) \quad \Omega = \{y_n > 0\}, \quad \partial\Omega = \{y_n = 0\}$$

locally around $y = 0$. Let $\mathbf{G} = (g_{ij})_{1 \leq i, j \leq n}$ be the metric tensor associated with the diffeomorphism $y = \Psi(x)$, whose components are given by

$$(2.2) \quad g_{ij} = \mathbf{e}_i \cdot \mathbf{e}_j.$$

Here the natural base related to the curvilinear coordinate system y is formed by

$$(2.3) \quad \mathbf{e}_i = \left[\frac{\partial x_k}{\partial y_i} \right]_{k \downarrow 1, 2, \dots, n} \quad (i = 1, 2, \dots, n).$$

We assume that $y = (y', y_n)$ forms the boundary normal coordinates so that

$$(2.4) \quad g_{nn} = 1, \quad g_{\alpha n} = g_{n\alpha} = 0 \quad (\alpha = 1, 2, \dots, n-1)$$

in a neighborhood of x_0 in $\bar{\Omega}$. The contravariant components g^{ij} ($1 \leq i, j \leq n$) of \mathbf{G}^{-1} are defined matrixwise as

$$(2.5) \quad (g^{ij}) = \mathbf{G}^{-1}.$$

Furthermore, it is easy to see that

$$(2.6) \quad g^{ij} = \sum_{k=1}^n \frac{\partial y_i}{\partial x_k} \frac{\partial y_j}{\partial x_k}.$$

It follows from (2.4) that in a neighborhood of x_0 in $\bar{\Omega}$ we have

$$(2.7) \quad g^{nn} = 1, \quad g^{\alpha n} = g^{n\alpha} = 0 \quad (\alpha = 1, 2, \dots, n-1).$$

Let d and δ be sufficiently small positive numbers so that the expressions (2.1) for Ω and $\partial\Omega$ are valid in a relatively open neighborhood \mathcal{N} of $x_0 \in \partial\Omega$, where

$$\mathcal{N} = \{ |y'| < d, \ 0 \leq y_n < 2\delta \} \subset \bar{\Omega}.$$

Let $\phi = \phi(y')$ be a phase function which satisfies the following eikonal equation:

$$(2.8) \quad \sum_{i,j=1}^{n-1} g^{ij}(y', 0) \frac{\partial \phi}{\partial y_i} \frac{\partial \phi}{\partial y_j} = 1.$$

We remark that equation (2.8) can be solved in $\{ |y'| < d \}$ by the method of characteristic curves ([13]). When $g^{ij}(y', 0) = \delta_{ij}$ ($i, j = 1, 2, \dots, n-1$), we immediately have $\phi = y' \cdot t'$, where $t' = (t_1, \dots, t_{n-1})$ is any unit vector in \mathbb{R}^{n-1} . We shall use this specific phase function below in our numerical experiments.

Theorem 1. *Suppose that $\gamma = \gamma(y', y_n)$ is a continuous function of $y_n \in [0, 2\delta]$ with values in the space of $L^2(\{|y'| \leq d\})$, and that $\nabla_{y'} \gamma(y', 0) \in L^2(\{|y'| \leq d\})$. Let $\eta(y')$ be any function in $C_0^1(\mathbb{R}^{n-1})$ compactly supported in $\{|y'| \leq d\}$ and define the Dirichlet data f_N and g_N for $N = 1, 2, 3, \dots$ by*

$$f_N = e^{iN\phi(y')} \eta(y') \Big|_{y=\Psi(x), x \in \partial\Omega}, \quad g_N = e^{i\frac{N}{2}\phi(y')} \eta(y') \Big|_{y=\Psi(x), x \in \partial\Omega}.$$

Then (i) and (ii) below hold:

(i) *We have the equality*

$$(2.9) \quad \lim_{N \rightarrow \infty} N^{-1} \langle \Lambda_\gamma f_N, \bar{f}_N \rangle = \int_{\mathbb{R}^{n-1}} \gamma(y', 0) \frac{\eta(y')^2}{\sqrt{\det(g^{ij}(y', 0))}} dy'.$$

- (ii) Assume that the diffeomorphism $y = \Psi(x)$ is C^2 . Suppose that $\gamma = \gamma(y', y_n)$ is a once continuously differentiable function of $y_n \in [0, 2\delta]$ with values in the space of $L^2(\{|y'| \leq d\})$, and that $\nabla_{y'} \gamma(y', 0) \in L^2(\{|y'| \leq d\})$. Then

$$(2.10) \quad \lim_{N \rightarrow \infty} \left[4 \langle \Lambda_\gamma g_N, \overline{g_N} \rangle - 2 \langle \Lambda_\gamma f_N, \overline{f_N} \rangle \right] = \int_{\mathbb{R}^{n-1}} \frac{\partial \gamma}{\partial y_n}(y', 0) \frac{\eta(y')^2}{\sqrt{\det(g^{ij}(y', 0))}} dy' \\ + \frac{1}{2} \int_{\mathbb{R}^{n-1}} \gamma(y', 0) \frac{\partial}{\partial y_n} \frac{\sum_{i,j=1}^{n-1} g^{ij} \phi_{y_i} \phi_{y_j} + 1}{\sqrt{\det(g^{ij})}} \Big|_{y_n=0} \eta(y')^2 dy'.$$

Proof of formulas (1.7) and (1.8). We remark that r, s and τ defined above satisfy the assumptions of the coordinate transformation in [30].

Putting $n = 3$ and $(y_1, y_2, y_3) = (y', y_3) = (\tau, s, r)$, from (2.3) and (1.4) we get

$$e_1 = \begin{bmatrix} 0 \\ 0 \\ 1 \end{bmatrix}, \quad e_2 = \begin{bmatrix} -(1 - \frac{r}{R}) \sin(\frac{s}{R}) \\ (1 - \frac{r}{R}) \cos(\frac{s}{R}) \\ 0 \end{bmatrix}, \quad e_3 = \begin{bmatrix} -\cos(\frac{s}{R}) \\ -\sin(\frac{s}{R}) \\ 0 \end{bmatrix}.$$

It can be seen from (2.2) and (2.5) that

$$\mathbf{G} = (g_{ij}) = \begin{bmatrix} 1 & 0 & 0 \\ 0 & (1 - r/R)^2 & 0 \\ 0 & 0 & 1 \end{bmatrix}, \quad (g^{ij}) = \begin{bmatrix} 1 & 0 & 0 \\ 0 & (1 - r/R)^{-2} & 0 \\ 0 & 0 & 1 \end{bmatrix}$$

and $\det(g^{ij}) = (1 - r/R)^{-2}$. We see that (τ, s, r) form boundary normal coordinates. Moreover, since $g^{ij}(y', 0) = \delta_{ij}$ ($i, j = 1, 2$), as a solution to eikonal equation (2.8) we may choose $\phi = y' \cdot t' = \tau t_1 + s t_2$, where $t' = (t_1, t_2)$ is any unit vector in \mathbb{R}^2 . Then formula (1.7) is an immediate consequence of formula (2.9).

Noting that $-\frac{\partial \gamma}{\partial(\tau)}(\tau, s, 0) = \frac{\partial \gamma}{\partial(\nu)}(\tau, s, 0)$, where ν is the outward unit normal vector to the boundary $\partial\Omega$, we obtain

$$\int_{\mathbb{R}^2} \frac{\partial \gamma}{\partial(\nu)}(\tau, s, 0) \eta(\tau, s)^2 d\tau ds = \lim_{N \rightarrow \infty} \left[2 \langle \Lambda_\gamma \phi_N, \overline{\phi_N} \rangle - 4 \langle \Lambda_\gamma \psi_N, \overline{\psi_N} \rangle \right] \\ - \frac{1 + t_1^2 - t_2^2}{2R} \int_{\mathbb{R}^2} \gamma(\tau, s, 0) \eta(\tau, s)^2 d\tau ds,$$

which combined with (1.7) yields (1.8).

3. PROOF OF THEOREM 1

Let $\zeta(y_n) \in C^\infty([0, \infty))$ satisfy $0 \leq \zeta \leq 1$, $\zeta(y_n) = 1$ for $0 \leq y_n \leq \delta$, and $\zeta(y_n) = 0$ for $2\delta \leq y_n$. Then from the weak formulation of Λ_γ it follows that

$$(3.1) \quad \langle \Lambda_\gamma f_N, \overline{f_N} \rangle = \int_{\Omega} \gamma \nabla u_N \cdot \nabla(\zeta \overline{F_N}) dx,$$

where $u_N \in H^1(\Omega)$ is the solution to

$$(3.2) \quad \nabla \cdot (\gamma \nabla u_N) = 0 \quad \text{in } \Omega, \quad u_N|_{\partial\Omega} = f_N,$$

and $F_N(x)$ is an $H^1(\Omega)$ extension of f_N , for which we take

$$(3.3) \quad F_N(x) = e^{iN\phi(y')} e^{-Ny_n} \eta(y') \Big|_{y=\Psi(x)}.$$

Put $r_N = u_N - \zeta F_N$. Then we get from (3.1)

$$\langle \Lambda_\gamma f_N, \overline{f_N} \rangle = \int_\Omega \gamma \nabla(\zeta F_N) \cdot \nabla(\zeta \overline{F_N}) dx + \int_\Omega \gamma \nabla r_N \cdot \nabla(\zeta \overline{F_N}) dx = I_1 + I_2.$$

It suffices to show that

$$(3.4) \quad \lim_{N \rightarrow \infty} N^{-1} I_1 = \int_{\mathbb{R}^{n-1}} \gamma(y', 0) \frac{\eta(y')^2}{\sqrt{\det(g^{ij}(y', 0))}} dy',$$

$$(3.5) \quad \lim_{N \rightarrow \infty} N^{-1} I_2 = 0.$$

We denote the Jacobian of the diffeomorphism $y = \Psi(x)$ by $\nabla \Psi$, which is given by

$$(3.6) \quad \nabla \Psi = \left(\frac{\partial y_i}{\partial x_j} \right)_{i \downarrow j \rightarrow 1, 2, \dots, n}.$$

Then $\nabla = \nabla_x = {}^t \nabla \Psi \nabla_y$, where the superscript t denotes transposition. By the change of the coordinate systems between x and y , integral I_1 becomes

$$(3.7) \quad \begin{aligned} I_1 &= \int_{\mathcal{N}} \gamma(y) {}^t \nabla \Psi \nabla_y(\zeta F_N) \cdot {}^t \nabla \Psi \nabla_y(\zeta \overline{F_N}) |\det \nabla \Psi|^{-1} dy \\ &= \int_{\mathcal{N}} \gamma(y) \left(\frac{\nabla \Psi {}^t \nabla \Psi}{|\det \nabla \Psi|} \nabla_y(\zeta F_N) \right) \cdot \nabla_y(\zeta \overline{F_N}) dy. \end{aligned}$$

Equations (2.6) and (3.6) imply that $|\det \nabla \Psi|^{-1} \nabla \Psi {}^t \nabla \Psi = (\det(g^{ij}))^{-1/2} (g^{ij})$. Henceforth, we use the $n \times n$ symmetric matrix $\tilde{\gamma}$

$$(3.8) \quad \tilde{\gamma}(y) = \gamma(y) (\det(g^{ij}))^{-1/2} (g^{ij}).$$

Then $I_1 = \int_{\mathcal{N}} \tilde{\gamma}(y) \nabla_y(\zeta F_N) \cdot \nabla_y(\zeta \overline{F_N}) dy$. Noting the support of ζF_N , we put $D = \{|y'| \leq d, 0 \leq y_n \leq \delta\}$ and $D' = \{|y'| \leq d, \delta \leq y_n\}$ to decompose I_1 as

$$(3.9) \quad I_1 = \int_D \tilde{\gamma}(y) \nabla_y F_N \cdot \nabla_y \overline{F_N} dy + \int_{D'} \tilde{\gamma}(y) \nabla_y(\zeta F_N) \cdot \nabla_y(\zeta \overline{F_N}) dy = I_3 + I_4.$$

Now (3.3) implies the following two equations:

$$(3.10) \quad \nabla_y F_N = \left(N \begin{bmatrix} i \nabla_{y'} \phi \\ -1 \end{bmatrix} \eta(y') + \begin{bmatrix} \nabla_{y'} \eta \\ 0 \end{bmatrix} \right) e^{i N \phi(y')} e^{-N y_n},$$

$$(3.11) \quad \nabla_y(\zeta F_N) = \left(N \begin{bmatrix} i \nabla_{y'} \phi \\ -1 \end{bmatrix} \zeta(y_n) \eta(y') + \nabla_y(\zeta \eta) \right) e^{i N \phi(y')} e^{-N y_n}.$$

Thus we see that $I_4 = O(N e^{-2\delta N})$ and

$$(3.12) \quad \begin{aligned} I_3 &= N^2 \int_D \tilde{\gamma}(y) \begin{bmatrix} i \nabla_{y'} \phi \\ -1 \end{bmatrix} \cdot \begin{bmatrix} -i \nabla_{y'} \phi \\ -1 \end{bmatrix} \eta(y')^2 e^{-2N y_n} dy \\ &\quad + \int_D \tilde{\gamma}(y) \begin{bmatrix} \nabla_{y'} \eta \\ 0 \end{bmatrix} \cdot \begin{bmatrix} \nabla_{y'} \eta \\ 0 \end{bmatrix} e^{-2N y_n} dy. \end{aligned}$$

In deriving (3.12), we have used the fact that the term of the order $O(N)$ in the integrand of I_3 vanishes, because

$$\tilde{\gamma}(y) \begin{bmatrix} \nabla_{y'} \eta \\ 0 \end{bmatrix} \cdot \begin{bmatrix} -i \nabla_{y'} \phi \\ -1 \end{bmatrix} + \tilde{\gamma}(y) \begin{bmatrix} i \nabla_{y'} \phi \\ -1 \end{bmatrix} \cdot \begin{bmatrix} \nabla_{y'} \eta \\ 0 \end{bmatrix} = \tilde{\gamma}(y) \begin{bmatrix} \nabla_{y'} \eta \\ 0 \end{bmatrix} \cdot \begin{bmatrix} 0 \\ -2 \end{bmatrix} = 0,$$

the last equality of which follows from (2.7) and (3.8).

After the scaling transformation $z_n = N y_n$ we get for large N

$$I_3 = N \int_0^{N\delta} \left(\int_{|y'| \leq d} \tilde{\gamma}(y', \frac{z_n}{N}) \begin{bmatrix} i \nabla_{y'} \phi \\ -1 \end{bmatrix} \cdot \begin{bmatrix} -i \nabla_{y'} \phi \\ -1 \end{bmatrix} \eta(y')^2 dy' \right) e^{-2z_n} dz_n + O\left(\frac{1}{N}\right).$$

The order of the last term in the right hand side follows from $\tilde{\gamma}(y) \in L^\infty(D)$ and $z_n = N y_n$. The dominated convergence theorem and $\int_0^\infty e^{-2z_n} dz_n = \frac{1}{2}$ imply

$$\lim_{N \rightarrow \infty} N^{-1} I_3 = \frac{1}{2} \int_{|y'| \leq d} \tilde{\gamma}(y', 0) \begin{bmatrix} i \nabla_{y'} \phi \\ -1 \end{bmatrix} \cdot \begin{bmatrix} -i \nabla_{y'} \phi \\ -1 \end{bmatrix} \eta(y')^2 dy'.$$

By (2.7) and (3.8), the integrand on the right hand side becomes

$$(3.13) \quad \gamma(y', 0) \left(\sum_{i,j=1}^{n-1} g^{ij}(y', 0) \frac{\partial \phi}{\partial y_i} \frac{\partial \phi}{\partial y_j} + 1 \right) \frac{\eta(y')^2}{\sqrt{\det(g^{ij}(y', 0))}}.$$

Therefore, from eikonal equation (2.8) we obtain

$$(3.14) \quad \lim_{N \rightarrow \infty} N^{-1} I_3 = \int_{|y'| \leq d} \gamma(y', 0) \frac{\eta(y')^2}{\sqrt{\det(g^{ij}(y', 0))}} dy'.$$

This, combined with (3.9) and $I_4 = O(Ne^{-2\delta N})$, proves (3.4).

To prove (3.5), we follow basically the methods in [7] and [35]. From (3.2), (3.3) and $r_N = u_N - \zeta F_N$ it follows that $r_N \in H_0^1(\Omega)$ satisfies $\nabla \cdot (\gamma \nabla r_N) = -\nabla \cdot (\gamma \nabla (\zeta F_N))$ in Ω . The Lax-Milgram theorem ([16], §§5.7, 5.8) implies that

$$(3.15) \quad \|r_N\|_{H_0^1(\Omega)} \leq C \|\nabla \cdot (\gamma \nabla (\zeta F_N))\|_{H^{-1}(\Omega)}.$$

Here and hereafter we denote by C any positive constants (depending on γ, Ψ, ζ or η) without distinguishing between them. We use the dual pairing of $H^{-1}(\Omega)$ with $H_0^1(\Omega)$ to write I_2 as $I_2 = -\langle \nabla \cdot (\gamma \nabla (\zeta F_N)), r_N \rangle_{H^{-1}-H_0^1}$. Then $|I_2| \leq \|\nabla \cdot (\gamma \nabla (\zeta F_N))\|_{H^{-1}(\Omega)} \|r_N\|_{H_0^1(\Omega)}$ and it follows from (3.15) that

$$(3.16) \quad |I_2| \leq C \|\nabla \cdot (\gamma \nabla (\zeta F_N))\|_{H^{-1}(\Omega)}^2.$$

Hence we shall estimate $\|\nabla \cdot (\gamma \nabla (\zeta F_N))\|_{H^{-1}(\Omega)}$.

For any $v \in H_0^1(\Omega)$, it follows after changing coordinates (see (3.6)–(3.8)) that

$$\begin{aligned} \langle \nabla \cdot (\gamma \nabla (\zeta F_N)), v \rangle_{H^{-1}-H_0^1} &= - \int_{\Omega} \gamma \nabla (\zeta F_N) \cdot \nabla v dx \\ &= - \int_{\mathcal{N}} \tilde{\gamma}(y) \nabla_y (\zeta F_N) \cdot \nabla_y v dy \\ &= - \int_{\mathcal{N}} \left(\tilde{\gamma}(y', y_n) - \tilde{\gamma}(y', 0) \right) \nabla_y (\zeta F_N) \cdot \nabla_y v dy - \int_{\mathcal{N}} \tilde{\gamma}(y', 0) \nabla_y (\zeta F_N) \cdot \nabla_y v dy \\ &= I_5(v) + I_6(v) \end{aligned}$$

for $v \in H_0^1(\Omega)$. Hence

$$(3.17) \quad \nabla \cdot (\gamma \nabla (\zeta F_N)) = I_5 + I_6, \quad I_5, I_6 \in H^{-1}(\Omega).$$

By the Schwarz inequality $|I_5(v)|^2 \leq C \int_{\mathcal{N}} |\tilde{\gamma}(y', y_n) - \tilde{\gamma}(y', 0)|^2 |\nabla_y (\zeta F_N)|^2 dy |v|_{H_0^1(\Omega)}^2$, and we get $\|I_5\|_{H^{-1}(\Omega)}^2 \leq C \int_{\mathcal{N}} |\tilde{\gamma}(y', y_n) - \tilde{\gamma}(y', 0)|^2 |\nabla_y (\zeta F_N)|^2 dy$. From (3.11) and

the scaling transformation $z_n = N y_n$ we have

$$\begin{aligned}
\|I_5\|_{H^{-1}(\Omega)}^2 &\leq C \int_0^{2\delta} \int_{|y'|\leq d} |\tilde{\gamma}(y', y_n) - \tilde{\gamma}(y', 0)|^2 \\
&\quad \times \left(N^2 (|\nabla_{y'}\phi|^2 + 1) \zeta(y_n)^2 \eta(y')^2 + O(N) \right) e^{-2Ny_n} dy' dy_n \\
&= C \int_0^{2N\delta} \int_{|y'|\leq d} |\tilde{\gamma}(y', \frac{z_n}{N}) - \tilde{\gamma}(y', 0)|^2 \\
(3.18) \quad &\quad \times \left(N (|\nabla_{y'}\phi|^2 + 1) \zeta\left(\frac{z_n}{N}\right)^2 \eta(y')^2 + O(1) \right) e^{-2z_n} dy' dz_n
\end{aligned}$$

for large N . Therefore, Lebesgue's dominated convergence theorem and the assumption in (i) of the theorem imply that

$$(3.19) \quad N^{-\frac{1}{2}} \|I_5\|_{H^{-1}(\Omega)} = 0 \quad (N \rightarrow +\infty).$$

Now we shall estimate $I_6(v)$. From (3.11) it follows that

$$\begin{aligned}
I_6(v) &= -N \int_{\mathcal{N}} \tilde{\gamma}(y', 0) \begin{bmatrix} i \nabla_{y'} \phi \\ -1 \end{bmatrix} \cdot \nabla_y v \zeta(y_n) \eta(y') e^{iN\phi(y')} e^{-Ny_n} dy \\
(3.20) \quad &- \int_{\mathcal{N}} \tilde{\gamma}(y', 0) \nabla_y (\zeta \eta) \cdot \nabla_y v e^{iN\phi(y')} e^{-Ny_n} dy = I_7(v) + I_8(v).
\end{aligned}$$

Since $v \in H_0^1(\Omega)$ and $\zeta(y_n) \eta(y') v = 0$ on $\partial\mathcal{N}$, integrating by parts leads to

$$\begin{aligned}
I_7(v) &= N \int_{\mathcal{N}} \left[\nabla_y \cdot \tilde{\gamma}(y', 0) \begin{bmatrix} i \nabla_{y'} \phi \\ -1 \end{bmatrix} \right] \zeta(y_n) \eta(y') e^{iN\phi(y')} e^{-Ny_n} v dy \\
&+ N \int_{\mathcal{N}} \tilde{\gamma}(y', 0) \begin{bmatrix} i \nabla_{y'} \phi \\ -1 \end{bmatrix} \cdot \nabla_y (\zeta \eta) e^{iN\phi(y')} e^{-Ny_n} v dy \\
&+ N^2 \int_{\mathcal{N}} \tilde{\gamma}(y', 0) \begin{bmatrix} i \nabla_{y'} \phi \\ -1 \end{bmatrix} \cdot \begin{bmatrix} i \nabla_{y'} \phi \\ -1 \end{bmatrix} \zeta(y_n) \eta(y') e^{iN\phi(y')} e^{-Ny_n} v dy.
\end{aligned}$$

The last integral on the right hand side vanishes, because (2.7), (3.8) and eikonal equation (2.8) imply that

$$\tilde{\gamma}(y', 0) \begin{bmatrix} i \nabla_{y'} \phi \\ -1 \end{bmatrix} \cdot \begin{bmatrix} i \nabla_{y'} \phi \\ -1 \end{bmatrix} = \frac{\gamma(y', 0)}{\sqrt{\det(g^{ij}(y', 0))}} \left(- \sum_{i,j=1}^{n-1} g^{ij}(y', 0) \phi_{y_i} \phi_{y_j} + 1 \right) = 0.$$

To estimate the first two terms on the right hand side, as in [7] and [35] we use the following consequence of Hardy's inequality [14]: $\|v/y_n\|_{L^2(\mathcal{N})} \leq 2\|\partial v/\partial y_n\|_{L^2(\mathcal{N})}$ for $v \in H_0^1(\Omega)$. Then it holds that

$$(3.21) \quad \left\| \frac{v}{y_n} \right\|_{L^2(\mathcal{N})} \leq C \|v\|_{H_0^1(\Omega)} \quad (v \in H_0^1(\Omega)).$$

Since $\nabla_{y'} \tilde{\gamma}(y', 0), \tilde{\gamma}(y', 0) \in L^2(\{|y'| \leq d\})$, the Schwarz inequality and (3.21) imply that

$$|I_7(v)| \leq CN \left(\|y_n \nabla_{y'} \tilde{\gamma}(y', 0) e^{-Ny_n}\|_{L^2(\mathcal{N})} + \|y_n \tilde{\gamma}(y', 0) e^{-Ny_n}\|_{L^2(\mathcal{N})} \right) \|v\|_{H_0^1(\Omega)},$$

and it follows from $z_n = N y_n$ that

$$(3.22) \quad |I_7(v)| \leq CN^{\frac{-1}{2}} \left(\|z_n \nabla_{y'} \tilde{\gamma}(y', 0) e^{-z_n}\|_{L^2(|y'| \leq d, 0 \leq z_n \leq 2N\delta)} \right. \\ \left. + \|z_n \tilde{\gamma}(y', 0) e^{-z_n}\|_{L^2(|y'| \leq d, 0 \leq z_n \leq 2N\delta)} \right) \|v\|_{H_0^1(\Omega)} \leq CN^{\frac{-1}{2}} \|v\|_{H_0^1(\Omega)}.$$

Here we have used the relation

$$(3.23) \quad \|\cdot\|_{L^2(\mathcal{N})} = N^{\frac{-1}{2}} \|\cdot\|_{L^2(|y'| \leq d, 0 \leq z_n \leq 2N\delta)}.$$

We get from the Schwarz inequality $|I_8(v)| \leq C \|\tilde{\gamma}(y', 0) e^{-N y_n}\|_{L^2(\mathcal{N})} \|v\|_{H_0^1(\Omega)}$ and from (3.23) we have $|I_8(v)| \leq CN^{\frac{-1}{2}} \|v\|_{H_0^1(\Omega)}$. Combining this with (3.20) and (3.22) we obtain

$$(3.24) \quad \|I_6\|_{H^{-1}(\Omega)} = O(N^{\frac{-1}{2}}) \quad (N \rightarrow +\infty).$$

Thus, from (3.17), (3.19) and (3.24) we have $\|\nabla \cdot (\gamma \nabla(\zeta F_N))\|_{H^{-1}(\Omega)} = o(N^{\frac{1}{2}})$. Hence from (3.16) we get $I_2 = o(N)$ as $N \rightarrow +\infty$. This proves (3.5).

Next we prove (ii). From the weak formulation of Λ_γ it follows that

$$(3.25) \quad 4\langle \Lambda_\gamma g_N, \overline{g_N} \rangle - 2\langle \Lambda_\gamma f_N, \overline{f_N} \rangle = \int_\Omega 4\gamma \nabla v_N \cdot \nabla(\zeta \overline{G_N}) - 2\gamma \nabla u_N \cdot \nabla(\zeta \overline{F_N}) \, dx.$$

Here $u_N \in H^1(\Omega)$ is the solution to (3.2), F_N is defined by (3.3), $v_N \in H^1(\Omega)$ is the solution to $\nabla \cdot (\gamma \nabla v_N) = 0$ in Ω with $v_N|_{\partial\Omega} = g_N$, and $G_N(x)$ is an $H^1(\Omega)$ extension of g_N , for which we choose $G_N(x) = e^{i\frac{N}{2}\phi(y')} e^{-\frac{N}{2}y_n} \eta(y')|_{y=\Psi(x)}$. Put $r_N = u_N - \zeta F_N$ and $s_N = v_N - \zeta G_N$. It follows that $r_N, s_N \in H_0^1(\Omega)$. Equation (3.25) can be written as

$$\begin{aligned} & 4\langle \Lambda_\gamma g_N, \overline{g_N} \rangle - 2\langle \Lambda_\gamma f_N, \overline{f_N} \rangle \\ &= \int_\Omega (4\gamma \nabla(\zeta G_N) \cdot \nabla(\zeta \overline{G_N}) - 2\gamma \nabla(\zeta F_N) \cdot \nabla(\zeta \overline{F_N})) \, dx \\ & \quad - 2 \int_\Omega \gamma \nabla r_N \cdot \nabla(\zeta \overline{F_N}) \, dx + 4 \int_\Omega \gamma \nabla s_N \cdot \nabla(\zeta \overline{G_N}) \, dx = J_1 - 2J_2 + 4J_3. \end{aligned}$$

We shall show that

$$(3.26) \quad \lim_{N \rightarrow \infty} J_1 = \int_{\mathbb{R}^{n-1}} \frac{\partial \gamma}{\partial y_n}(y', 0) \frac{\eta(y')^2}{\sqrt{\det(g^{ij}(y', 0))}} \, dy' \\ + \frac{1}{2} \int_{\mathbb{R}^{n-1}} \gamma(y', 0) \frac{\partial}{\partial y_n} \frac{\sum_{i,j=1}^{n-1} g^{ij} \phi_{y_i} \phi_{y_j} + 1}{\sqrt{\det(g^{ij})}} \Big|_{y_n=0} \eta(y')^2 \, dy'$$

and $\lim_{N \rightarrow \infty} J_2 = 0$ and $\lim_{N \rightarrow \infty} J_3 = 0$.

As in the proof of (i), after the change of the coordinate system, using the regions D and D' in (3.9) we write J_1 as

$$(3.27) \quad J_1 = \int_D (4 \tilde{\gamma}(y) \nabla_y G_N \cdot \nabla_y \overline{G_N} - 2 \tilde{\gamma}(y) \nabla_y F_N \cdot \nabla_y \overline{F_N}) \, dy, \\ + \int_{D'} (4 \tilde{\gamma}(y) \nabla_y(\zeta G_N) \cdot \nabla_y(\zeta \overline{G_N}) - 2 \tilde{\gamma}(y) \nabla_y(\zeta F_N) \cdot \nabla_y(\zeta \overline{F_N})) \, dy \\ = J_4 + J_5.$$

From (3.10), (3.11),

$$\nabla_y G_N = \left(\frac{N}{2} \begin{bmatrix} i \nabla_{y'} \phi \\ -1 \end{bmatrix} \eta(y') + \begin{bmatrix} \nabla_{y'} \eta \\ 0 \end{bmatrix} \right) e^{i \frac{N}{2} \phi(y')} e^{-\frac{N}{2} y_n},$$

and

$$\nabla_y (\zeta G_N) = \left(\frac{N}{2} \begin{bmatrix} i \nabla_{y'} \phi \\ -1 \end{bmatrix} \zeta(y_n) \eta(y') + \nabla_y (\zeta \eta) \right) e^{i \frac{N}{2} \phi(y')} e^{-\frac{N}{2} y_n}$$

it follows that $J_5 = O(Ne^{-\delta N})$ and

$$\begin{aligned} J_4 &= N^2 \int_D \tilde{\gamma}(y) \begin{bmatrix} i \nabla_{y'} \phi \\ -1 \end{bmatrix} \cdot \begin{bmatrix} -i \nabla_{y'} \phi \\ -1 \end{bmatrix} \eta(y')^2 (e^{-N y_n} - 2e^{-2N y_n}) dy \\ (3.28) \quad &+ 2 \int_D \tilde{\gamma}(y) \begin{bmatrix} \nabla_{y'} \eta \\ 0 \end{bmatrix} \cdot \begin{bmatrix} \nabla_{y'} \eta \\ 0 \end{bmatrix} (2e^{-N y_n} - e^{-2N y_n}) dy. \end{aligned}$$

Integration by parts applied to the first integral on the right hand side of (3.28), combined with $e^{-N y_n} - e^{-2N y_n}|_{y_n=0}$, implies that the first term becomes

$$N \int_0^\delta \int_{|y'| \leq d} \frac{\partial \tilde{\gamma}}{\partial y_n} \begin{bmatrix} i \nabla_{y'} \phi \\ -1 \end{bmatrix} \cdot \begin{bmatrix} -i \nabla_{y'} \phi \\ -1 \end{bmatrix} \eta(y')^2 dy' (e^{-N y_n} - e^{-2N y_n}) dy_n + O(Ne^{-\delta N})$$

for large N . Then after the scaling transformation $z_n = N y_n$ we get for large N

$$\begin{aligned} J_4 &= \int_0^{N\delta} \left(\int_{|y'| \leq d} \frac{\partial \tilde{\gamma}}{\partial y_n} \left(y', \frac{z_n}{N} \right) \begin{bmatrix} i \nabla_{y'} \phi \\ -1 \end{bmatrix} \cdot \begin{bmatrix} -i \nabla_{y'} \phi \\ -1 \end{bmatrix} \eta(y')^2 dy' \right) \\ &\quad \times (e^{-z_n} - e^{-2z_n}) dz_n + O(N^{-1}). \end{aligned}$$

Lebesgue's bounded convergence theorem and $\int_0^\infty (e^{-z_n} - e^{-2z_n}) dz_n = \frac{1}{2}$ imply

$$\lim_{N \rightarrow \infty} J_4 = \frac{1}{2} \int_{|y'| \leq d} \frac{\partial \tilde{\gamma}}{\partial y_n} (y', 0) \begin{bmatrix} i \nabla_{y'} \phi \\ -1 \end{bmatrix} \cdot \begin{bmatrix} -i \nabla_{y'} \phi \\ -1 \end{bmatrix} \eta(y')^2 dy'.$$

From (3.8) we have

$$\frac{\partial \tilde{\gamma}}{\partial y_n} (y', 0) = \frac{\partial \gamma}{\partial y_n} (y', 0) \frac{(g^{ij}(y', 0))}{\sqrt{\det(g^{ij}(y', 0))}} + \gamma(y', 0) \frac{\partial}{\partial y_n} \frac{(g^{ij})}{\sqrt{\det(g^{ij})}} \Big|_{y_n=0}.$$

Recalling that

$$(g^{ij}(y', 0)) \begin{bmatrix} i \nabla_{y'} \phi \\ -1 \end{bmatrix} \cdot \begin{bmatrix} -i \nabla_{y'} \phi \\ -1 \end{bmatrix} = 2$$

which follows from (2.7) and (2.8) (cf. (3.13) and (3.14)), we obtain

$$\begin{aligned} \lim_{N \rightarrow \infty} J_4 &= \int_{|y'| \leq d} \frac{\partial \gamma}{\partial y_n} (y', 0) \frac{\eta(y')^2}{\sqrt{\det(g^{ij}(y', 0))}} dy' \\ &\quad + \frac{1}{2} \int_{|y'| \leq d} \gamma(y', 0) \frac{\partial}{\partial y_n} \frac{\sum_{i,j=1}^{n-1} g^{ij} \phi_{y_i} \phi_{y_j} + 1}{\sqrt{\det(g^{ij})}} \Big|_{y_n=0} \eta(y')^2 dy' \end{aligned}$$

This, combined with (3.27) and $J_5 = O(Ne^{-\delta N})$, proves (3.26).

To prove $\lim_{N \rightarrow \infty} J_2 = 0$ and $\lim_{N \rightarrow \infty} J_3 = 0$, recalling that we already have

$$(3.29) \quad |J_2| \leq C \|\nabla \cdot (\gamma \nabla (\zeta F_N))\|_{H^{-1}(\Omega)}^2$$

(see (3.16)), we shall estimate $\|\nabla \cdot (\gamma \nabla (\zeta F_N))\|_{H^{-1}(\Omega)}$ under the conditions in (ii) of the theorem. For any $v \in H_0^1(\Omega)$, as in (3.17) we can write

$$(3.30) \quad \nabla \cdot (\gamma \nabla (\zeta F_N)) = J_6 + J_7,$$

where $J_6, J_7 \in H^{-1}(\Omega)$ and

$$\begin{aligned} J_6(v) &= - \int_{\mathcal{N}} \left(\tilde{\gamma}(y', y_n) - \tilde{\gamma}(y', 0) \right) \nabla_y(\zeta F_N) \cdot \nabla_y v \, dy, \\ J_7(v) &= - \int_{\mathcal{N}} \tilde{\gamma}(y', 0) \nabla_y(\zeta F_N) \cdot \nabla_y v \, dy. \end{aligned}$$

Then $\|J_6\|_{H^{-1}(\Omega)}$ has the estimate (3.18) for large N . We get now for almost every y' the identity $\tilde{\gamma}(y', y_n) - \tilde{\gamma}(y', 0) = \int_0^{y_n} \frac{\partial \tilde{\gamma}}{\partial y_n}(y', \theta_n) \, d\theta_n$. Hence

$$\left| \tilde{\gamma}(y', \frac{z_n}{N}) - \tilde{\gamma}(y', 0) \right|^2 = \left| \int_0^{\frac{z_n}{N}} \frac{\partial \tilde{\gamma}}{\partial y_n}(y', \theta_n) \, d\theta_n \right|^2 \leq \frac{z_n}{N} \int_0^{\frac{z_n}{N}} \left| \frac{\partial \tilde{\gamma}}{\partial y_n}(y', \theta_n) \right|^2 \, d\theta_n.$$

Substituting this, we have

$$\begin{aligned} \|J_6\|_{H^{-1}(\Omega)}^2 &\leq C \int_0^{2N\delta} \frac{z_n}{N} \int_{|y'| \leq d} \int_0^{\frac{z_n}{N}} \left| \frac{\partial \tilde{\gamma}}{\partial y_n}(y', \theta_n) \right|^2 \, d\theta_n \\ &\quad \times (N(|\nabla_{y'} \phi|^2 + 1) \eta(y')^2 + O(1)) e^{-2z_n} \, dy' \, dz_n, \end{aligned}$$

and from Fubini's theorem and the assumption we get for large N

$$\begin{aligned} \|J_6\|_{H^{-1}(\Omega)}^2 &\leq C \int_0^{2N\delta} z_n \int_0^{\frac{z_n}{N}} \int_{|y'| \leq d} \left| \frac{\partial \tilde{\gamma}}{\partial y_n}(y', \theta_n) \right|^2 \\ &\quad \times ((|\nabla_{y'} \phi|^2 + 1) \eta(y')^2 + O(N^{-1})) \, dy' \, d\theta_n \, e^{-2z_n} \, dz_n \\ &\leq C \max_{\theta_n \in [0, 2\delta]} \int_{|y'| \leq d} \left| \frac{\partial \tilde{\gamma}}{\partial y_n}(y', \theta_n) \right|^2 (|\nabla_{y'} \phi|^2 + 1) \eta(y')^2 \, dy' \\ &\quad \times \int_0^{2N\delta} z_n \cdot \frac{z_n}{N} (1 + O(N^{-1})) e^{-2z_n} \, dz_n. \end{aligned}$$

Consequently we can estimate J_6 as follows:

$$\begin{aligned} \|J_6\|_{H^{-1}(\Omega)} &\leq CN^{-1/2} \left(\max_{\theta_n \in [0, 2\delta]} \int_{|y'| \leq d} \left| \frac{\partial \tilde{\gamma}}{\partial y_n}(y', \theta_n) \right|^2 (|\nabla_{y'} \phi|^2 + 1) \eta(y')^2 \, dy' \right. \\ &\quad \left. \times \int_0^\infty z_n^2 e^{-2z_n} \, dz_n \right)^{\frac{1}{2}} + O(N^{-1}). \end{aligned}$$

Therefore we obtain $\|J_6\|_{H^{-1}(\Omega)} = O(N^{-\frac{1}{2}})$. The proof of $\|J_7\|_{H^{-1}(\Omega)} = O(N^{-\frac{1}{2}})$ is exactly the same as that of (3.24). These estimates together with (3.30) imply

$$\|\nabla \cdot (\gamma \nabla(\zeta F_N))\|_{H^{-1}(\Omega)} = O(N^{-\frac{1}{2}}) \quad (N \rightarrow +\infty).$$

Therefore, from (3.29) we get $J_2 = O(N^{-1})$ as $N \rightarrow +\infty$. This proves $\lim_{N \rightarrow \infty} J_2 = 0$. The proof of $\lim_{N \rightarrow \infty} J_3 = 0$ is parallel.

4. SIMULATION OF MEASUREMENT DATA

4.1. Solution of the boundary value problem with FEM. We need a variational equation for approximating the solution of (1.1) with FEM. We use test

functions $v \in H^1(\Omega)$ and denote $H = H^1(\Omega) \times \mathbb{R}^L$. Multiplying (1.1) with a test function and integrating over the domain Ω yields

$$(4.1) \quad \int_{\Omega} v \nabla \cdot (\gamma \nabla u) \, dx = 0.$$

Equation (4.1) is referred to as the *variational form* of (1.1), and using Green's formula we can write it in the form

$$(4.2) \quad \int_{\Omega} \gamma \nabla u \cdot \nabla v \, dx - \int_{\partial\Omega} \gamma \frac{\partial u}{\partial \nu} v \, dS = 0.$$

The domain Ω is discretized into small tetrahedral elements and the potential distribution u in Ω is expressed as linear combination of piecewise linear basis functions φ_j $j = 1, \dots, K$:

$$(4.3) \quad u(x) \approx \sum_{j=1}^K u_j \varphi_j(x), \quad x \in \mathbb{R}^3.$$

Here K is the number of nodal points x_j in the finite element mesh and $u_j = u(x_j)$. The piecewise linear basis functions $\varphi_j \in H^1(\Omega)$ are constructed uniquely by the requirement $\varphi_j(x_\ell) = \delta_{j\ell}$; we denote $E_j := \text{supp}(\varphi_j) \subset \Omega$.

Inserting the approximation (4.3) into (4.2) and using the basis functions φ_j as test functions (Galerkin FEM scheme) yields

$$(4.4) \quad \sum_{k=1}^K u_k \int_{\Omega} \gamma \nabla \varphi_k \cdot \nabla \varphi_j \, dx - \sum_{k=1}^K u_k \int_{\partial\Omega} \gamma \frac{\partial \varphi_k}{\partial \nu} \varphi_j \, dS = 0.$$

This can be written in the matrix form

$$(4.5) \quad Au = 0$$

where the matrix A is defined as

$$(4.6) \quad A(k, j) = \int_{E_k \cup E_j} \gamma \nabla \varphi_k \cdot \nabla \varphi_j \, dx - \int_{\partial(E_k \cup E_j) \cap \partial\Omega} \gamma \frac{\partial \varphi_k}{\partial \nu} \varphi_j \, dS$$

and $u = [u_1, \dots, u_K]^T$. The solution of $Au = 0$ is not unique, but using the Dirichlet boundary condition $u = \phi_N$ on $x \in \partial\Omega$ and $u = 0$ on the horizontal boundaries (top and bottom) we can write

$$(4.7) \quad \tilde{A}\tilde{u} = -A_{\tilde{\phi}}\tilde{\phi}_N,$$

where $A_{\tilde{\phi}}$ includes the columns of the matrix A that correspond with the nodes on the lateral and horizontal boundaries, $\tilde{A} = A \setminus A_{\tilde{\phi}}$, $\tilde{\phi}_N = (\phi_N, \mathbf{0})$, $\mathbf{0} = (0, \dots, 0)^T \in \mathbb{R}^M$, M is the number of the nodes on the horizontal boundaries and $\tilde{u} = u \setminus \tilde{\phi}_N$. The problem (4.7) is overdetermined so the rows that correspond with the nodes at the boundary $\partial\Omega$ can be eliminated from the matrices \tilde{A} and $A_{\tilde{\phi}}$, resulting in a solvable linear system of equations.

Due to the above reduction, the boundary integrals in (4.6) need not to be computed. The integrations over tetrahedra in equation (4.6) are computed by using the mapping which relates the actual element (global) to a standard element, see [38]. We represent the conductivity distribution using piecewise linear basis.

Our local reconstruction method involves applying rather oscillatory Dirichlet data supported in small subsets of the boundary. Hence, in order to achieve an adequate accuracy with reasonable computational cost, it is advantageous to use

non-uniform finite element meshes with higher density near the support of the Dirichlet data. One example of a non-uniform mesh of the type we use is illustrated in Figure 1.

4.2. Choosing cut-off functions. We use the cut-off function $\eta(\tau, s) = \eta_1(s)\eta_2(\tau)$ with

$$(4.8) \quad \eta_1(s) = \begin{cases} c_1 (T - \frac{\pi R}{2\epsilon_2})^2 (T + \frac{\pi R}{2\epsilon_2})^2 & \text{for } -\frac{\pi R}{2\epsilon_2} < T < \frac{\pi R}{2\epsilon_2}, \\ 0 & \text{otherwise,} \end{cases}$$

$$(4.9) \quad \eta_2(\tau) = \begin{cases} c_2 (Z - \frac{\pi R}{2\epsilon_1})^2 (Z + \frac{\pi R}{2\epsilon_1})^2 & \text{for } -\frac{\pi R}{2\epsilon_1} < Z < \frac{\pi R}{2\epsilon_1}, \\ 0 & \text{otherwise,} \end{cases}$$

where $T = s - t$ and $s, t \in [0, 2\pi R]$ and $Z = \tau - z$ and $\tau, z \in [0, h]$. The constants c_j are chosen so that $\int \eta_j^2(s) ds = 1$ for $j = 1, 2$, and the parameters ϵ_1 and ϵ_2 can be used to adjust the width of the functions η_1 and η_2 .

Figure 2 shows the cut-off functions corresponding to different ϵ_1 and ϵ_2 in cylindrical geometry (1.3) with $R = 1$ and $h = 1.7671$.

4.3. Simulating noisy voltage-to-current measurements. We apply the Dirichlet data specified by the theory and calculate the potentials in inner nodes as a solution of the boundary value problem as explained in Section 4.1.

We evaluate the normal derivative of the potentials $\frac{\partial u}{\partial \nu}$ for the computation of the current density. Gradient of u can be approximated as follows: In the case of piecewise linear basis functions the gradient ∇u is constant in each element and discontinuous on element boundaries. We estimate the value of the gradient in boundary nodes as a mean value of the all elements connected to the node in question. The normal derivative of the potentials in each node $(\tau, s, 0)$ on the lateral surface of Ω can be then computed from the equation

$$(4.10) \quad \frac{\partial u}{\partial \nu}(\tau, s, 0) = \nabla u(\tau, s, 0) \cdot \nu(\tau, s, 0).$$

We add simulated measurement noise \mathcal{E}_N to the computed current density.

$$(4.11) \quad \mathcal{E}_N = \sum_{l=-N+1}^N \sigma a_l e^{il\theta},$$

where a_l are independent normally distributed random variables with mean zero and standard deviation 1, and $\sigma > 0$ is a constant used to tune the noise amplitude.

5. NUMERICAL EXPERIMENTS

In this section we test the reconstruction formulas (1.7) and (1.8) numerically with a sequence of three-dimensional conductivity distributions with increasing complexity. As difficulties arise, we design corrective steps to overcome them. This process leads to a novel noise-robust reconstruction algorithm that is presented in detail in Section 6.

For a given conductivity γ we define

$$(5.1) \quad \tilde{g}_N := \frac{1}{N} \int_{\mathbb{R}^2} \overline{\phi_N} \Lambda_\gamma \phi_N d\tau ds.$$

As the surface measure on the lateral boundary Γ is $d\tau ds$, by formula (1.7) we have $\tilde{g}_N \approx \int_{\mathbb{R}^2} \gamma(\tau, s, 0) \eta(\tau, s)^2 d\tau ds$. Furthermore, set

$$(5.2) \quad \tilde{h}_N := \left(2 + \frac{t_2^2 - t_1^2 - 1}{2NR}\right) \int_{\mathbb{R}^2} \overline{\phi_N} \Lambda_\gamma \phi_N d\tau ds - 4 \int_{\mathbb{R}^2} \overline{\psi_N} \Lambda_\gamma \psi_N d\tau ds.$$

for any unit vector (t_1, t_2) . Then by formula (1.8) we have

$$\tilde{h}_N \approx \int_{\mathbb{R}^2} \frac{\partial \gamma}{\partial \nu}(\tau, s, 0) \eta(\tau, s)^2 d\tau ds.$$

We work in cylindrical geometry (1.3) with $R = 1$ and $h = 1.7671$. We use standard deviation $\sigma = 0.0001$ in (4.11), giving relative noise level 0.01 %.

5.1. Homogeneous conductivity. Our first experiment uses simply the homogeneous conductivity distribution $\gamma_0 \equiv 1$. We substitute Λ_{γ_0} to formula (1.7) and call the result $\tilde{g}_N^{(0)}$. Then we have $\tilde{g}_N^{(0)} \rightarrow 1$ as N grows, and we can study numerically the speed of convergence using various values of the related parameters.

Let us first get an idea how large N is practically useful. Figure 3 shows the Dirichlet data for several values of N . Apparently there is hope of representing the data with $N = 20$ with 64 electrodes in a 8×8 configuration, but the data with $N = 50$ seems to need way too many electrodes to be practically feasible. This rough derivation is based on the simple idea that each minimum and maximum of the Dirichlet data needs to be evaluated on at least one electrode. Consequently we will restrict our experiments to $0 < N \leq 50$.

Next we examine the convergence rate $\tilde{g}_N^{(0)} \rightarrow 1$ as N grows. Figure 4 shows $\tilde{g}_N^{(0)}$ as function of N computed with finite element mesh with varying numbers of elements. We conclude that the mesh comprising 9324 nodes gives acceptable accuracy in the range $14 \leq N \leq 20$, and we will use that mesh in the sequel.

We study the effect of cut-off function on speed of convergence by choosing different values for ϵ_1 and ϵ_2 in (4.8) and (4.9), respectively. Figure 5 illustrates that using a wider cut-off function leads to faster convergence. Thus there is a trade-off between (a) more accurate reconstruction using a narrow cut-off function that better approximates Dirac's delta, and (b) higher rate of convergence.

We proceed to test the reconstruction of the normal derivative. We substitute Λ_{γ_0} to formula (1.8) and call the result $\tilde{h}_N^{(0)}$. Then by formula (1.8) we have $\tilde{h}_N^{(0)} \rightarrow 0$ as $N \rightarrow \infty$. Line “* *” in Figure 6 shows $\tilde{h}_N^{(0)}$ as function of N . We see that $\tilde{h}_N^{(0)}$ converges slowly and the apparent limit value is -5 instead of the value 0 predicted by theory. We conclude that more experimenting is needed to find out what's going on.

5.2. Radial conductivities with unit trace. We define a collection of radially varying conductivity distributions for further testing of formula (5.2):

$$\begin{aligned} \gamma_1(\tau, s, r) &:= R - r, & \gamma_1|_{\partial\Omega} &= 1, & \frac{\partial \gamma_1}{\partial \nu}|_{\partial\Omega} &= 1, \\ \gamma_2(\tau, s, r) &:= (R - r)^2, & \gamma_2|_{\partial\Omega} &= 1, & \frac{\partial \gamma_2}{\partial \nu}|_{\partial\Omega} &= 2, \\ \gamma_3(\tau, s, r) &:= (R - r)^3, & \gamma_3|_{\partial\Omega} &= 1, & \frac{\partial \gamma_3}{\partial \nu}|_{\partial\Omega} &= 3. \end{aligned}$$

Figure 6 shows the convergence of \tilde{h}_N as function of N computed using formula (5.2) for γ_1 and γ_2 and γ_3 . We see that the various \tilde{h}_N converge slowly to limit values with systematic error of -5 .

However, the evidence in Figure 6 suggests the *relative* values of \tilde{h}_N are roughly correct throughout the computational interval $2 \leq N \leq 20$! This surprising observation can be used to calibrate the results as follows. Suppose we have available measurements Λ_{γ_0} from the “dummy load” conductivity $\gamma_0 \equiv 1$. We can compute $\tilde{h}_{20}^{(0)} \approx -5$ corresponding to γ_0 . Since the relative values of \tilde{h}_N are close to correct for γ_1 and γ_2 and γ_3 , we suggest that the formula

$$(5.3) \quad \frac{\partial \gamma}{\partial \nu}(x_0) \approx \tilde{h}_{20}(x_0) - \tilde{h}_{20}^{(0)}(x_0)$$

serves as a calibrated reconstruction method of the normal derivative for any conductivity γ with trace 1.

We remark that recovering the traces of γ_1 and γ_2 and γ_3 using formula (5.1) works with similar accuracy and convergence properties as for γ_0 in Section 5.1 despite the different normal derivatives.

5.3. Radial conductivities with varying traces. It remains to study the numerical properties of formula (5.2) in the case of conductivities whose trace is not 1. To this end, we define a collection of conductivities with varying traces as follows:

$$\begin{aligned} \gamma_4(\tau, s, r) &:= R - r + 1, & \gamma_4|_{\partial\Omega} &= 2, & \frac{\partial \gamma_4}{\partial \nu}|_{\partial\Omega} &= 1, \\ \gamma_5(\tau, s, r) &:= R - r + 2, & \gamma_5|_{\partial\Omega} &= 3, & \frac{\partial \gamma_5}{\partial \nu}|_{\partial\Omega} &= 1, \\ \gamma_6(\tau, s, r) &:= R - r + 3, & \gamma_6|_{\partial\Omega} &= 4, & \frac{\partial \gamma_6}{\partial \nu}|_{\partial\Omega} &= 1. \end{aligned}$$

The integral in formula (5.1) as function of N is shown in Figure 7. The slope of the curve increases when conductivity value on the boundary node increases; the values of the integral actually seem to depend linearly on the conductivity value at the boundary. For instance, for fixed N , the integral corresponding to γ_4 satisfying $\gamma_4(\tau, s, 0) = 2$ is twice as large as the integral corresponding to γ_1 satisfying $\gamma_1(\tau, s, 0) = 1$.

Same phenomenon can be found when normal derivatives are estimated, see Fig. 8. Hence we suggest that $\tilde{h}_{20}^{(0)}$ in calibrated algorithm (5.3) should be multiplied by estimated conductivity $\tilde{g}_{20}(x_0)$.

$$(5.4) \quad \frac{\partial \gamma}{\partial \nu}(\tau, s) \approx \tilde{h}_{20}(x_0) - \tilde{h}_{20}^{(0)}(x_0) \tilde{g}_{20}(x_0).$$

6. THE CALIBRATED RECONSTRUCTION ALGORITHM

The numerical experiments presented in Section 5 inspire us to suggest the following calibrated method for recovering the trace and normal derivative of a given conductivity γ based on localized boundary measurements.

- (1) Use the dummy load $\gamma_0 \equiv 1$ to find a big enough $N_0 > 0$ for $\tilde{g}_{N_0}^{(0)}$ computed by formula (1.7) to be reasonably close to 1.
- (2) Use formula (1.7) to recover $\gamma|_{\Gamma}$ approximately as $\gamma(\tau, s, 0) \approx \tilde{g}_{N_0}(\tau, s)$.
- (3) Substitute the dummy load to formula (1.8) and denote the result by $\tilde{h}_{N_0}^{(0)}$.

(4) Use formula (1.7) to recover the normal derivative of γ approximately as

$$\frac{\partial \gamma}{\partial \nu}(\tau, s) \approx \tilde{h}_{N_0}(\tau, s) - \tilde{h}_{N_0}^{(0)}(\tau, s) \tilde{g}_{N_0}(\tau, s).$$

We tested the calibrated reconstruction algorithm with the simple cases discussed in Section 5. Figure 9 shows the calibrated normal derivatives for the radial conductivities with unit trace as function of N . The bigger change in conductivity in the normal direction the smaller gets the current density on the boundary in the case of finite N . Hence the integral in formula (5.1) gets smaller values even if the trace of the conductivity on the boundary is same in all cases. Therefore the calibrated algorithm (5.4) underestimates the normal derivatives of the conductivity.

Figure 10 shows the calibrated normal derivatives for the radial conductivities with varying trace as function of N . As can be seen from the Table 1, absolute error between true conductivity and its convolution increases when conductivity value increases. Therefore also error in calibrated normal derivative of the conductivity increases with the conductivity value.

TABLE 1. Absolute errors and relative errors for the reconstruction of $\gamma|_{\partial\Omega}$.

	$ \gamma - \gamma * \eta^2 _{N=20}$	$\frac{ \gamma - \gamma * \eta^2 _{N=20}}{\gamma}$	$\min \frac{ \gamma - \gamma * \eta^2 }{\gamma}$
$\gamma_1(\tau, s, 0) = 1$	0.0915	0.0915	0.0074
$\gamma_2(\tau, s, 0) = 2$	0.1844	0.0922	0.0079
$\gamma_3(\tau, s, 0) = 3$	0.2661	0.0887	0.0154
$\gamma_4(\tau, s, 0) = 4$	0.3479	0.0870	0.0166

At the moment the approximation properties of the above method are not well understood. However, we can gather intuition about the method by testing it also with a more demanding example. We test our calibrated reconstruction algorithm with a fairly complicated non-homogeneous distribution with three inclusions. Two of the inclusions touch the boundary and one is located in the middle of the target, see Figure 11.

We estimate the conductivity and normal derivatives on 1216 boundary points (64 equidistantly placed points on 19 layers). A nonuniform finite element mesh is constructed corresponding to each boundary point; the number of nodes in the meshes is on the average 9000. See Figure 12 for the recovered trace and Figure 13 for the approximate normal derivative reconstructed using the above calibration.

We computed the relative $L^2(\partial\Omega)$ and $L^\infty(\partial\Omega)$ errors between true conductivity distribution $\gamma|_{\partial\Omega}$ and its convolution $\gamma * \eta^2$. Errors were computed also between $\gamma * \eta^2$ and its approximation \tilde{g}_N .

$$(6.1) \quad E_\gamma^2 = \frac{\|\gamma - \gamma * \eta^2\|_{L^2(\partial\Omega)}}{\|\gamma\|_{L^2(\partial\Omega)}} \quad E_\gamma^\infty = \frac{\max_{\partial\Omega} |\gamma - \gamma * \eta^2|}{\max_{\partial\Omega} |\gamma|}$$

$$(6.2) \quad E_g^2(N) = \frac{\|\tilde{g}_N - \gamma * \eta^2\|_{L^2(\partial\Omega)}}{\|\gamma\|_{L^2(\partial\Omega)}} \quad E_g^\infty(N) = \frac{\max_{\partial\Omega} |\tilde{g}_N - \gamma * \eta^2|}{\max_{\partial\Omega} |\gamma|}$$

See Tables 2 for reconstruction errors.

TABLE 2. Relative errors (6.1) and (6.2) for the convolution and reconstruction of $\gamma|_{\partial\Omega}$. Three lowest and three highest boundary node layers have been removed.

E_γ^2	E_γ^∞	$E_g^2(N)$	$E_g^\infty(N)$
0.0149	0.1009	0.0242	0.0384

7. CONCLUSION

Our study of recovering trace and normal derivative of conductivity from static electric boundary measurements is based on two aspects: theoretical and numerical. Theoretically, we show that it is possible to recover convolved approximations to both trace and normal derivative from localized boundary measurements. Our Theorem 1 is proved under quite general geometric assumptions.

Our numerical experiments suggest that the trace of conductivity can be approximately recovered using Theorem 1 with a finite value of N and simulated data with realistic noise level. The recovery of the normal derivative seems to be more difficult, but we are able to introduce a calibration method allowing useful reconstructions at least for our simulated examples.

The applicability of our method for real-world measured data needs a further study. However, the voltage distributions applied at the boundary in our simulations seem to be representable using a 8×8 electrode array covering the support of the localized excitation pattern. Since we included simulated data with realistic noise level (relative error of the same order than in the ACT3 impedance imager of Rensselaer Polytechnic Institute [11]), we have a reason to believe that our method is implementable with a 64-channel impedance tomography device.

8. ACKNOWLEDGEMENTS

The work of KT was partly supported by Grant-in-Aid for Scientific Research (C) (No. 19540113), Society for the Promotion of Science, Japan. The work of SS was supported by the Finnish Centre of Excellence in Inverse Problems Research (Academy of Finland CoE-project 213476). During part of the preparation of this work, SS worked as professor at the Department of Mathematics of Tampere University of Technology.

REFERENCES

- [1] Alessandrini G 1990 *Singular solutions of elliptic equations and the determination of conductivity by boundary measurements* J Diff Eq **84** 252–273
- [2] Bikowski J 2008 *Electrical Impedance Tomography reconstructions in two and three dimensions; From Calderón to Direct Methods*, PhD Thesis, Colorado State University
- [3] R. Blue. *Real-time three-dimensional electrical impedance tomography*. PhD thesis, R.P.I., Troy, NY, 1997.
- [4] Borcea L 2002, *Electrical Impedance Tomography*, Inverse Problems **18** R99–R136.
- [5] Borcea L 2002, Addendum to “Electrical Impedance Tomography”, Inverse Problems **19** 997–998.
- [6] Boverman G, Isaacson D, Kao T-J, Saulnier G J and Newell J C 2008 *Methods for Direct Image Reconstruction for EIT in Two and Three Dimensions* *Proceedings of the 2008 Electrical Impedance Tomography Conference took place at Dartmouth College, in Hanover, New Hampshire, USA, June 16 to 18, 2008*
- [7] Brown R M, *Recovering the conductivity at the boundary from the Dirichlet to Neumann map: a pointwise result*, J. Inverse and Ill-posed Prob. **9** (2001)567-574.

- [8] Calderón A P 1980, On an inverse boundary value problem In *Seminar on Numerical Analysis and its Applications to Continuum Physics*, Soc. Brasileira de Matemática 65–73.
- [9] Cheney M, Isaacson D and Newell J C 1999, *Electrical Impedance Tomography* SIAM Review **41** 85–101.
- [10] Cheng K-S, Isaacson D, Newell J C and Gisser D G 1989, *Electrode models for electric current computed tomography* IEEE Transactions on Biomedical Imaging 918–924.
- [11] Cook R D, Saulnier G J and Goble J C 1991, *A phase sensitive voltmeter for a high-speed, high-precision electrical impedance tomograph* in Proc. Annu. Int. Conf. IEEE Engineering in Medicine and Biology Soc., 1991, pp. 22–23.
- [12] Cornean H, Knudsen K and Siltanen S 2006, *Towards a d-bar reconstruction method for three-dimensional EIT* Journal of Inverse and Ill-Posed Problems **14**(2), pp. 111–134.
- [13] R. Courant and D. Hilbert, *Methods of Mathematical Physics*, Interscience Publishers, Vol. II, 1962.
- [14] E. B. Davies, *Heat Kernels and Spectral Theory*, Cambridge University Press, 1989, Cambridge.
- [15] Gebauer B and Hyvönen N 2008 Factorization method and inclusions of mixed type in an inverse elliptic boundary value problem *Inverse Probl. Imaging* **2** 355–372
- [16] D. Gilbarg and N. S. Trudinger, *Elliptic Partial Differential Equations of Second Order*, Grundlehren der Mathematischen Wissenschaften Vol 224, Springer, 1989, Berlin.
- [17] J. Goble, M. Cheney, and D. Isaacson 1992. *Electrical impedance tomography in three dimensions*. Appl Comput Electromagn Soc J, **7** 128–147.
- [18] Hanke M and Schappel B 2008 The Factorization Method for Electrical Impedance Tomography in the Half-Space *SIAM J. Appl. Math.* **68** 907-924
- [19] T Ide, H Isozaki, S Nakata and S Siltanen *Local detection of three-dimensional inclusions in electrical impedance tomography* submitted manuscript
- [20] Isaacson D, Mueller J L, Newell J C and Siltanen S 2004, Reconstructions of chest phantoms by the d-bar method for electrical impedance tomography, to appear in IEEE Transactions on Medical Imaging.
- [21] Kang H and Yun K 2003, Boundary determination of conductivities and Riemannian metrics via local Dirichlet-to-Neumann operator, *SIAM J. Math. Anal.* **34** 719-735.
- [22] Kohn R V and Vogelius M 1984 Determining conductivity by boundary measurements *Commun. Pure Appl. Math.* **37** 289–298
- [23] Kohn R V and Vogelius M 1985 Determining conductivity by boundary measurements II. Interior results. *Commun. Pure Appl. Math.* **38** 643–667
- [24] P. Metherall, D.C. Barber, and R.H. Smallwood 1995, Three dimensional electrical impedance tomography. In Proc IX Int Conf Electrical Bio-Impedance, 510–511, Heidelberg, Germany.
- [25] P. Metherall, D.C. Barber, R.H. Smallwood, and B.H. Brown 1996. Three-dimensional electrical impedance tomography. *Nature*, **380** 509–512.
- [26] P. Metherall, R.H. Smallwood, and D.C. Barber 1996. Three dimensional electrical impedance tomography of the human thorax. In Proc 18th Int Conf IEEE Eng Med Biol Society.
- [27] J.P. Morucci, M. Granie, M. Lei, M. Chabert, and P.M. Marsili 1995. 3D reconstruction in electrical impedance imaging using a direct sensitivity matrix approach. *Physiol Meas*, **16** A123–A128.
- [28] Nachman A I 1988 Reconstructions from boundary measurements *Ann. of Math.* **128** 531–576
- [29] A. I. Nachman, Global uniqueness for a two-dimensional inverse boundary value problem, *Ann. of Math.* **143** (1996), pp. 71–96.
- [30] Nakamura G and Tanuma K 2001, Local determination of conductivity at the boundary from the Dirichlet-to-Neumann map, *Inverse Problems* **17** 405-419
- [31] Nakamura G and Tanuma K 2001, Direct determination of the derivatives of conductivity at the boundary from the localized Dirichlet to Neumann map, *Comm. Korean Math. Soc.* **16** 415-425.
- [32] Nakamura G and Tanuma K 2003, Formulas for reconstructing conductivity and its normal derivative at the boundary from the localized Dirichlet to Neumann map, in *Recent Development in Theories & Numerics, International Conference on Inverse Problems*, Yiu-Chung Hon, Masahiro Yamamoto, Jin Cheng and June-Yub Lee (eds.), World Scientific, 192-201
- [33] Nakamura G, Tanuma K, Siltanen S and Wang S, Numerical recovery of conductivity at the boundary from the localized Dirichlet to Neumann map, *Computing* **75**(2-3), pp. 197–213.

- [34] J. C. Newell, R. S. Blue, D. Isaacson, G. J. Saulnier, and A. S. Ross. Phasic three-dimensional impedance imaging of cardiac activity. *Physiol. Meas.* **23** (2002), 203–209.
- [35] R. L. Robertson, Boundary identifiability of residual stress via the Dirichlet to Neumann map, *Inverse Problems* **13** (1997) 1107–1119.
- [36] Somersalo E, Cheney M and Isaacson D 1992, Existence and uniqueness for electrode models for electric current computed tomography, *SIAM J. Appl. Math.* **52** 1023–1040.
- [37] Sylvester J and Uhlmann G 1988 *Inverse boundary value problems at the boundary — continuous dependence* *Comm Pure Appl Math* **41** 197–221
- [38] Vauhkonen P J 2004 Image Reconstruction in Three-Dimensional Electrical Impedance Tomography, Phd thesis, University of Kuopio.
- [39] P.J. Vauhkonen, M. Vauhkonen, T. Savolainen, and J.P. Kaipio 1999. Static three-dimensional electrical impedance tomography. *Ann New York Acad Sci*, **873** 472–481.
- [40] P.J. Vauhkonen, M. Vauhkonen, T. Savolainen, and J.P. Kaipio 1999. Three-dimensional electrical impedance tomography based on the complete electrode model. *IEEE Trans Biomed Eng.* **46** 1150–1160.
- [41] Wexler A 1988 Electrical impedance imaging in two and three dimensions. *Clin Phys Physiol Meas, Suppl A*, **929–33**.

1 GRADUATE SCHOOL OF SCIENCE, HOKKAIDO UNIVERSITY, JAPAN

2 DEPARTMENT OF PHYSICS, UNIVERSITY OF KUOPIO, FINLAND

3 DEPARTMENT OF MATHEMATICS AND STATISTICS, UNIVERSITY OF HELSINKI, FINLAND

4 DEPARTMENT OF MATHEMATICS, GRADUATE SCHOOL OF ENGINEERING, GUNMA UNIVERSITY, JAPAN

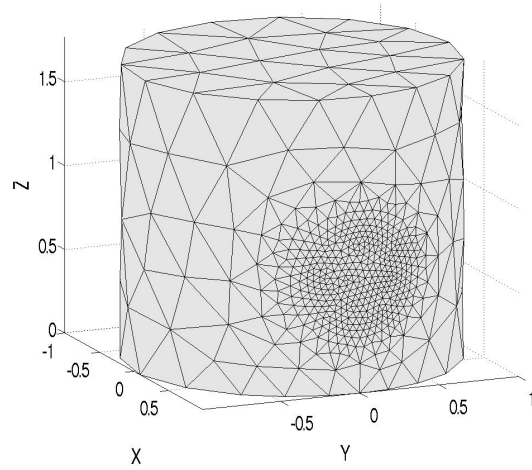


FIGURE 1. Computational grid corresponding to one boundary node. Number of the nodes is 950.

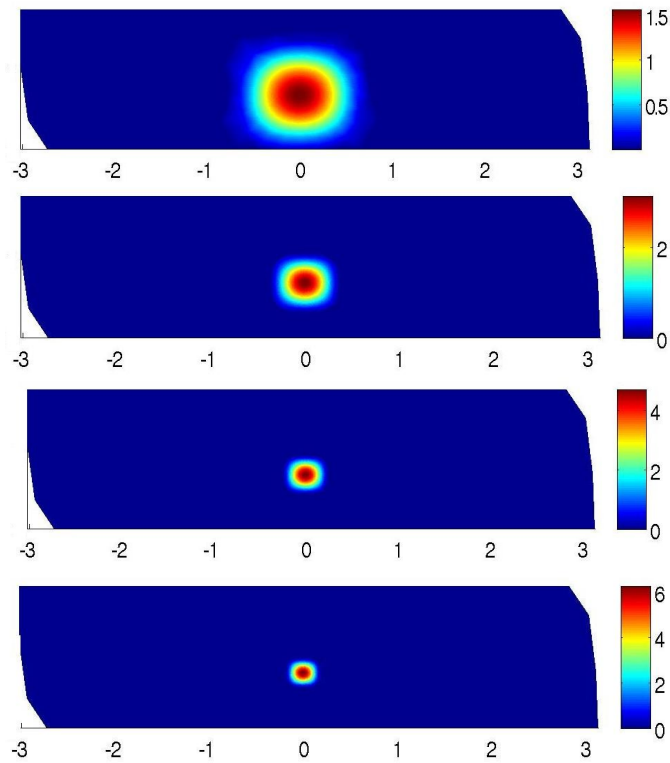


FIGURE 2. Plot of the cut-off function $\eta(\tau, s)$ with various ϵ_1 and ϵ_2 . First row: $\epsilon_1 = \epsilon_2 = 2$. Second row: $\epsilon_1 = \epsilon_2 = 4$. Third row: $\epsilon_1 = \epsilon_2 = 6$. Fourth row: $\epsilon_1 = \epsilon_2 = 8$.

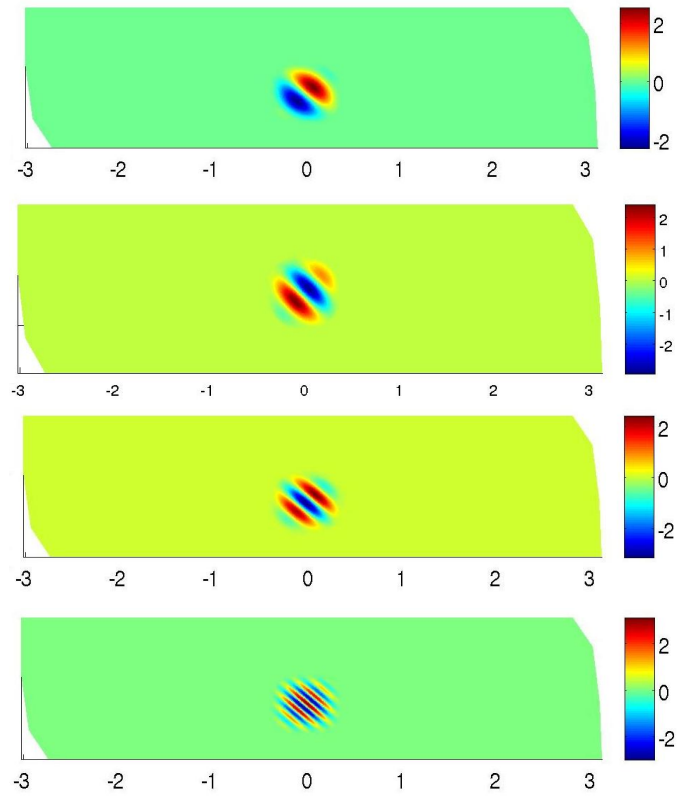


FIGURE 3. Plot of the Dirichlet data ϕ_N with three different values of N . $t_1 = t_2 = \frac{1}{\sqrt{2}}$ and $\epsilon_1 = \epsilon_2 = 4$. First row: $N = 10$. Second row: $N = 14$. Third row: $N = 20$. Fourth row: $N = 50$

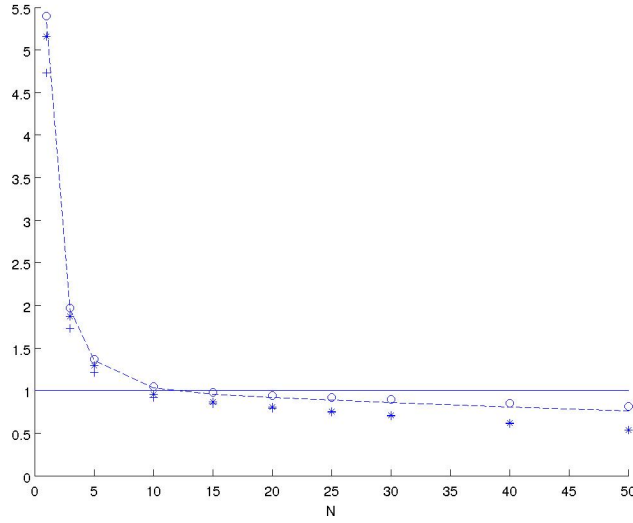


FIGURE 4. Estimated convolution \tilde{g}_N as a function of N corresponding to one node on the boundary with different computational grids, $\epsilon_1 = \epsilon_2 = 4$. Correct value of conductivity is one. Line “* * *”: 950 nodes in grid. Line “+ + +”: 2946 nodes in grid. Line “- -”: 9324 nodes in grid. Line “o o”: 16285 nodes in grid.

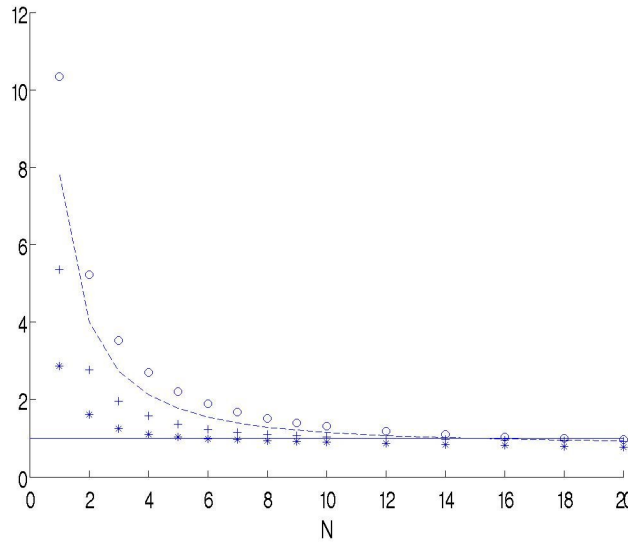


FIGURE 5. Estimated convolution \tilde{g}_N computed with formula (5.1) as a function of N corresponding to one node on the boundary with computational grid of 9324 nodes and various ϵ_1 and ϵ_2 . Correct value of conductivity is one. Line “* * *”: $\epsilon_1 = \epsilon_2 = 2$. Line “+ + +”: $\epsilon_1 = \epsilon_2 = 4$. Line “- -”: $\epsilon_1 = \epsilon_2 = 6$. Line “o o”: $\epsilon_1 = \epsilon_2 = 8$.

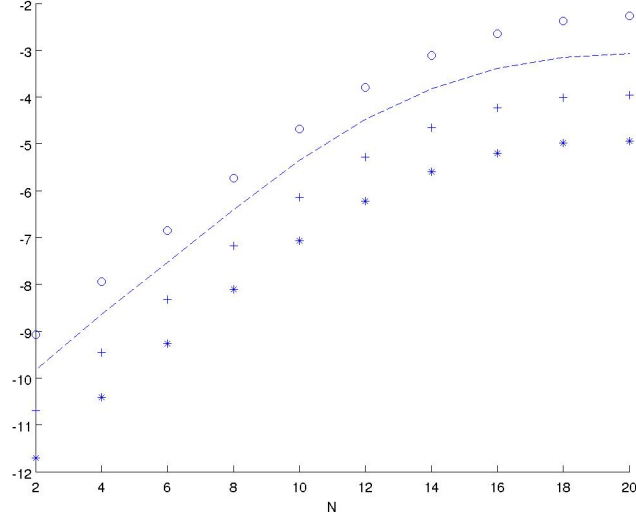


FIGURE 6. Estimated normal derivative \tilde{h}_N computed with formula (5.2) as a function of N corresponding to one node on the boundary: computational grid of 9324 nodes, $R = 1$ and $\epsilon_1 = \epsilon_2 = 4$. Line “* * ”: $\gamma_0(\tau, s, r) = 1$ and $\frac{\partial \gamma_0}{\partial \nu}|_{\partial \Omega} = 0$. Line “+ + ”: $\gamma_1(\tau, s, r) = R - r$ and $\frac{\partial \gamma_1}{\partial \nu}|_{\partial \Omega} = 1$. Line “- - ”: $\gamma_2(\tau, s, r) = (R - r)^2$ and $\frac{\partial \gamma_2}{\partial \nu}|_{\partial \Omega} = 2$. Line “o o ”: $\gamma_3(\tau, s, r) = (R - r)^3$ and $\frac{\partial \gamma_3}{\partial \nu}|_{\partial \Omega} = 3$.

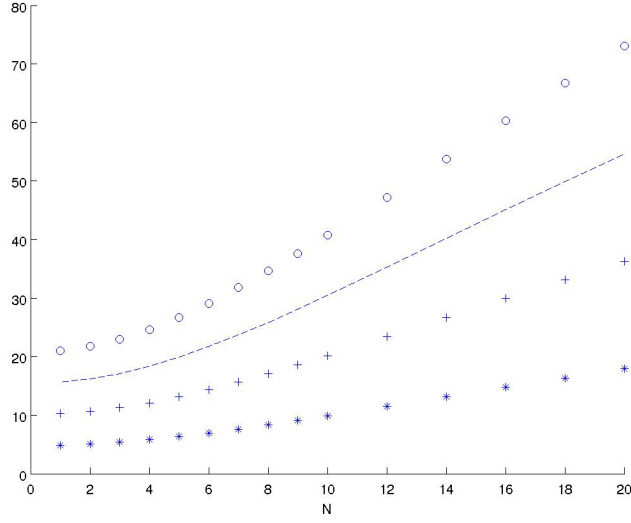


FIGURE 7. The values of the integral in formula (5.1) as a function of N corresponding to one node on the boundary with computational grid of 9324 nodes, $R = 1$ and $\epsilon_1 = \epsilon_2 = 4$. Line “* *”: conductivity distribution $\gamma_1(\tau, s, r) = R - r$, on the boundary $\gamma_1(\tau, s, 0) = 1$. Line “+ +”: conductivity distribution $\gamma_4(\tau, s, r) = (R - r) + 1$, on the boundary $\gamma_4(\tau, s, 0) = 2$. Line “- -”: conductivity distribution $\gamma_5(\tau, s, r) = (R - r) + 2$, on the boundary $\gamma_5(\tau, s, 0) = 3$. Line “o o”: conductivity distribution $\gamma_6(\tau, s, r) = (R - r) + 3$, on the boundary $\gamma_6(\tau, s, 0) = 4$.

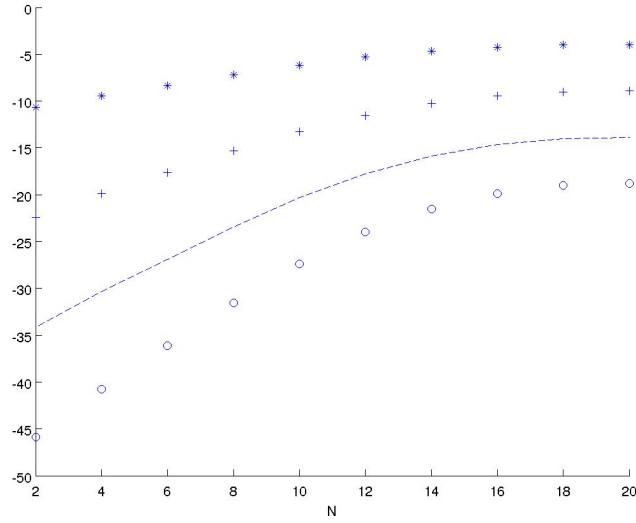


FIGURE 8. Estimated normal derivative \tilde{h}_N computed with formula (5.2) as a function of N corresponding to one node on the boundary for the conductivity distributions: computational grid of 9324 nodes, $R = 1$ and $\epsilon_1 = \epsilon_2 = 4$. Line “* *”: $\gamma_1(\tau, s, r) = R - r$ and $\frac{\partial \gamma_1}{\partial \nu}|_{\partial \Omega} = 1$. Line “+ +”: $\gamma_4(\tau, s, r) = (R - r) + 1$ and $\frac{\partial \gamma_4}{\partial \nu}|_{\partial \Omega} = 1$. Line “- -”: $\gamma_5(\tau, s, r) = (R - r) + 2$ and $\frac{\partial \gamma_5}{\partial \nu}|_{\partial \Omega} = 1$. Line “o o”: $\gamma_6(\tau, s, r) = (R - r) + 3$ and $\frac{\partial \gamma_6}{\partial \nu}|_{\partial \Omega} = 1$.

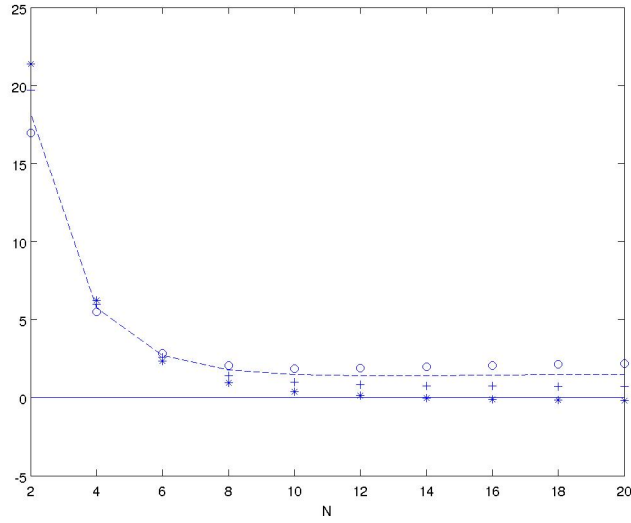


FIGURE 9. Calibrated normal derivative computed with formula (5.4) as a function of N corresponding to one node on the boundary: computational grid of 9324 nodes, $R = 1$ and $\epsilon_1 = \epsilon_2 = 4$. Line “*”: $\gamma_0(\tau, s, r) = 1$ and $\frac{\partial \gamma_0}{\partial \nu}|_{\partial \Omega} = 0$. Line “+ +”: $\gamma_1(\tau, s, r) = R - r$ and $\frac{\partial \gamma_1}{\partial \nu}|_{\partial \Omega} = 1$. Line “- -”: $\gamma_2(\tau, s, r) = (R - r)^2$ and $\frac{\partial \gamma_2}{\partial \nu}|_{\partial \Omega} = 2$. Line “o o”: $\gamma_3(\tau, s, r) = (R - r)^3$ and $\frac{\partial \gamma_3}{\partial \nu}|_{\partial \Omega} = 3$.

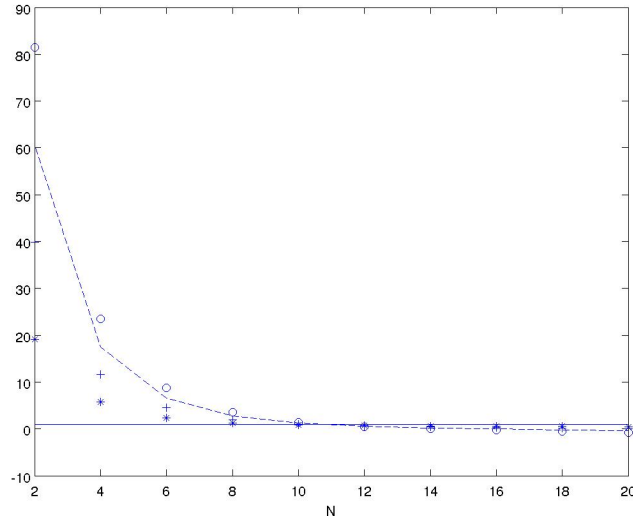


FIGURE 10. Calibrated normal derivative computed with formula (5.4) as a function of N corresponding to one node on the boundary for the conductivity distributions: computational grid of 9324 nodes, $R = 1$ and $\epsilon_1 = \epsilon_2 = 4$. Line “* *”: $\gamma_1(\tau, s, r) = R - r$ and $\frac{\partial \gamma_1}{\partial \nu} |_{\partial \Omega} = 1$. Line “+ +”: $\gamma_4(\tau, s, r) = (R - r) + 1$ and $\frac{\partial \gamma_4}{\partial \nu} |_{\partial \Omega} = 1$. Line “- -”: $\gamma_5(\tau, s, r) = (R - r) + 2$ and $\frac{\partial \gamma_5}{\partial \nu} |_{\partial \Omega} = 1$. Line “o o”: $\gamma_6(\tau, s, r) = (R - r) + 3$ and $\frac{\partial \gamma_6}{\partial \nu} |_{\partial \Omega} = 1$.

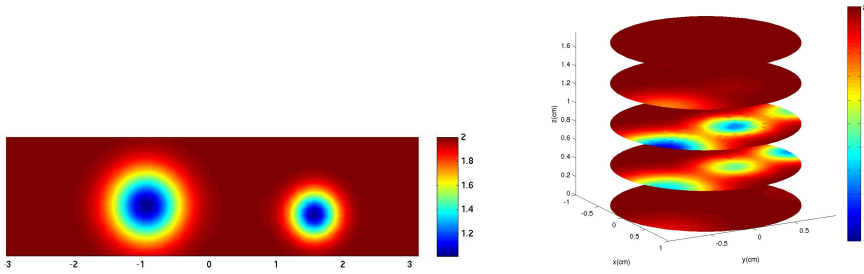


FIGURE 11. Left: true conductivity distribution on the lateral boundary. Right: The conductivity distribution on five cross-sectional planes.

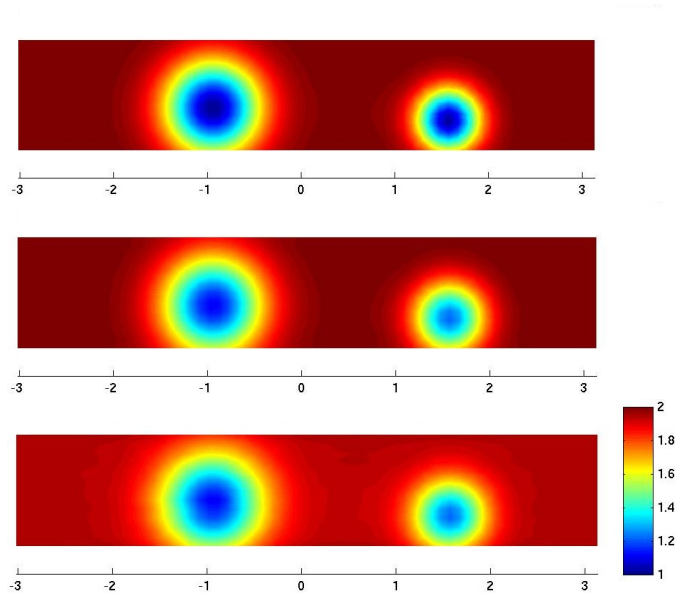


FIGURE 12. True conductivity distribution $\gamma(\tau, s, 0)$ (first row), convolution $(\gamma|_{\partial\Omega} * \eta^2)(\tau, s)$ (second row) and estimated conductivity distribution \tilde{g}_N (third row) with same colormap.

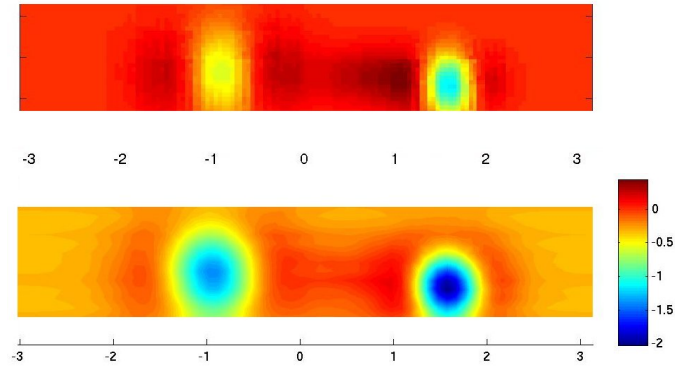


FIGURE 13. True normal derivative $\frac{\partial\gamma}{\partial\nu}(\tau, s, 0)$ (first row) and estimated normal derivative \tilde{h}_N (second row) with same colormap.